EXPERIMENTAL INVESTIGATION OF THE INTERACTION OF FLUID TRANSIENTS WITH AN IN-LINE AIR POCKET

Jane M. Alexander[1], Pedro J. Lee[2], Mark Davidson[3], Zhao Li[4], Ross Murch[5], Huan-Feng Duan[6], Silvia Meniconi[7], and Bruno Brunone[8]

[1]Ph.D. Student, Department of Civil and Natural Resources Engineering, College of Engineering, University of Canterbury, Private Bag 4800, Christchurch 8020, New Zealand. Email: jane.alexander@pg.canterbury.ac.nz

[2, 3]Professor, Department of Civil and Natural Resources Engineering, College of Engineering, University of Canterbury, Christchurch 8020, New Zealand.

[4]Research Fellow, Department of Civil and Natural Resources Engineering, College of Engineering, University of Canterbury, Christchurch 8020, New Zealand.

[5]Professor, Department of Electronic and Computer Engineering, Hong Kong University of Science and Technology, Clear Water Bay, Kowloon, Hong Kong.

[6]Associate Professor, Department of Civil and Environmental Engineering, The Hong Kong Polytechnic University, Hung Hom, Kowloon, Hong Kong.

[7]Associate Professor, Dipartimento di Ingegneria Civile ed Ambientale, Università degli Studi di Perugia, Perugia, Italy.

[8]Professor, Dipartimento di Ingegneria Civile ed Ambientale, Università degli Studi di Perugia, Perugia, Italy.

ABSTRACT

Entrapped air blocking the flow in pipeline systems is a common cause of increased pumping costs. At present, air is generally removed via valves or pipeline excavation and drilling. This becomes inefficient in large networks where the precise location of the air is unknown. Fluid transients are a potential tool for detecting and locating air in pipelines. The effect of a stationary air pocket part of the way along the pipe which occupies the main flow path and acts as a blockage without causing a hydraulic jump or column separation has not previously been studied experimentally. This paper presents experimental results for a transient pulse interacting with an in-line air pocket for a range of pocket sizes and system pressures. In accordance with impedance theory, the reflective power of the air increases with pocket size. Other notable characteristics of the interaction include frequency dependent transmissivity, an out-of-phase reflection, and a substantial reflection under zero base flow. These effects set air pockets apart from solid blockages, allowing a transient detection methodology to differentiate between the two cases although they have similar effects at steady state.

INTRODUCTION

A safe and reliable water supply is essential to supporting the health and sanitation of communities all over the world, as well as generating significant economic benefits. Functional water supply has become an expected service in developed nations, with significant investments required to install and maintain the associated infrastructure. During the period 2009 to 2019, New Zealand's operational expenditure for supplying public drinking water was estimated at NZ$65 million per year, with a capital expenditure of NZ$390 million per year (Auditor-General 2010). An integral part of modern water supply systems is pipelines. To most efficiently manage networks, regular condition assessment is required to diagnose anomalies. The ideal method will provide information about the type and the location of the anomaly, enabling a targeted repair or removal plan. Non-invasive testing methods are preferred as this will minimise cost and disruption to the system.

Entrapped air in a pipeline is a common issue and can pose a range of problems for network operators. Dissolved air exists naturally in water, with the amount of dissolution dependent on temperature and pressure. Water used in civil engineering applications contains approximately 2% air (Lauchlan et al. 2005), which may leave solution due to low pressure regions created by pump action or local turbulence, creating tiny bubbles which coalesce to form accumulated pockets (Young 1999). Other mechanisms by which air can enter pipelines include through pipe filling

(Lee 1991), as a byproduct of biological activity (National Research Council 1982), through joints, fittings, and leaks (Spellman 2013), or via transfer from surge control devices (Lauchlan et al. 2005). Under steady state conditions, accumulated in-line air reduces the pipe cross-section, causing a flow restriction and resulting in increased head loss, energy consumption, and ultimately pumping cost, similar to a solid blockage. Pozos et al. (2010) found that pumping accounts for approximately 75% of the operating costs of a distribution network, and entrapped air can reduce the overall efficiency by 30%. If left unchecked, the gradual growth of the pocket could cripple the operation of the system, particularly for undulating networks. Air pockets can also compromise system resilience, as their presence may exacerbate the transient pressures experienced during water hammer effects (Lauchlan et al. 2005). When the air cannot be easily swept downstream or bled through a valve, expensive and intrusive methods such as pipeline excavation or drilling vents at pipe high points may be required.

Fluid transients are a potential non-invasive tool for the detection and characterisation of pipeline faults, including trapped air pockets. When a transient wave encounters a flow anomaly, such as an air pocket, it is divided into reflected and transmitted components. If the impact of that particular anomaly on the reflection and transmission of the pulse is understood, measuring the evolution of pressure in the pipe after the controlled generation of a transient wave could allow the anomaly to be located and characterised. It is particularly useful to be able to differentiate between different flow-blocking elements, as in many cases air can be cheaply flushed out by changing the flow regime, whereas the removal of solid blockages or faulty valves invariably requires excavation.

The majority of the existing experimental investigations into the air-transient interaction focus on air pockets trapped at the end of a dead-end pipe, acted upon by a compression wave. Ocasio (1976) found that entrapped dead-end air could lead to extreme surges following an instantaneous valve opening. In the field, Jönsson (1985) observed that, for an air pocket trapped next to a valve, smaller equilibrium air volumes led to faster oscillations and larger transient peaks. Experiments by Lee and Martin (1999) and Lee (2005) for dead-end pockets ranging between 3% and 44.8% of the total pipe volume agreed with this observation. However, for the largest pocket volumes tested, the peak pressures were smaller than those obtained for the no air case, though a physical reasoning is not provided for this observation. Vasconcelos and Leite (2012) reached a similar conclusion for the case of a dead-end air pocket with base flow, while Lai et al. (2000) found that the peak pressures experienced are also influenced by the percentage of air in the void. Zhou (2000) presented experimental and observational studies into the case of an air pocket at the end of a pipe, adjacent to an orifice which allows limited air release. Large pockets were displaced and compressed by the transient wave, while smaller pockets were forced out the adjacent orifice. For smaller air volumes, the peak pressures increased as the cushioning effect of the air decreased. Zhou et al. (2011) found that for dead-end air volumes below approximately 0.05% of the total pipe volume peak pressures begin to decrease again, as below this threshold there is limited space for water column movement and hence a decrease in the water impact force.

The case of a stationary air pocket in the middle of the pipe has not been investigated to the same extent. Cabrera et al. (1992), Izquierdo et al. (1999), and Fuertes et al. (1999) carried out numerical investigations, using the rigid column model, into the case of system start-up when long columns of air are trapped in an undulating pipeline, entirely blocking the pipe cross-section. Pozos (2007) successfully utilised a linear equation to identify locations where air would gather in experimental systems, confirming the theory that air gravitates to and becomes fixed at high points. Pozos-Estrada (2017) carried out laboratory experiments to verify the open channel flow model for large in-line pockets followed by a hydraulic jump, finding that the presence of the pocket reduces the amplitude of transmitted pressure oscillations. To investigate the scenario of smaller pocket volumes which do not create a hydraulic jump, Kim (2008) carried out a set of experiments and numerical investigations for a range of air pocket volumes located at the pipe mid-point for a range of initial hydrostatic pressures and base flow velocities. The air pocket was isolated inside a brass block adjacent to the flow, meaning that the air was outside the main flow path (off-line) rather than in-line with flow. The air pocket was found to result in major changes to the shape and magnitude of the incident compression wave compared to the no-air case, with the air pocket creating high frequency pressure drops due to the sudden drop in fluid density. These changes were strongly dependent on the pocket volume and pressure condition. The advantage of the brass block approach is that the air is isolated outside the main flow path, so the effects of base flow can be investigated without risk of the air being swept elsewhere by the flow.

The purpose of this study is to carry out experimental investigations into the reflection and transmission of a rapid transient through an in-line air pocket for a range of air volumes and initial hydrostatic pressures. This complements other studies by Kim (2008) and Pozos-Estrada (2017) for discrete air pockets located part of the way along the pipe for the cases where the air pocket was off-line, or large enough to cause a hydraulic jump. A greater knowledge of the observable effects of this form of air on an incident transient wave would assist in the development of a fault detection framework, as this is a common scenario compromising the efficiency of supply networks (Lauchlan et al. 2005). The experimental results will be used to identify the effects of the in-line air pocket on a transient pulse. Some of the effects of air pockets at steady state, such as a reduced flow rate or increased pumping cost, are shared with other flow-constricting faults such as solid blockages and partially closed valves, but air pockets may be significantly cheaper to remove once identified. This means it is particularly useful to identify effects on the transient which are unique to air pockets.

EXPERIMENTAL PROCEDURE

The experiments were conducted at the University of Canterbury Fluids Laboratory using the experimental apparatus shown in Fig. 1. The system consisted of a downstream reservoir capable of being pressurised up to 3.0 bar, a 41.6 m steel pipeline with a 22.25 mm internal diameter, and a closed solenoid valve located at the upstream end of the pipe, 14.50 m from the air pocket location. The solenoid valve was adjacent to the upstream reservoir which is not pressurised. The pipe was set at a constant angle of 3.5°, resulting in a height difference of 2.51 m between the two ends of the pipe. A steel test section containing a crest was inserted into the pipeline at the location shown in Fig. 1. Air was inserted into the test section via a bleed valve using a plastic measuring syringe which allowed the volume of air, V, at atmospheric pressure to be measured before insertion. The air was also extracted and measured using the syringe at the end of each test to ensure no air had moved elsewhere in the pipe. To measure the transient pressure disturbances, PCB Piezotronics Model 102A07 dynamic pressure transducers with a sampling frequency of 10,000 Hz were installed along the pipe at four locations. The transducers have a 345 kPa measuring range, a natural frequency of over 250 kHz, and an uncertainty of 3.45 kPa. PT1 was located at the transient generation point at the end of the pipe, 14.50 m upstream of the air pocket. PT2 was located 8.29 m downstream of the transient generation point, 6.21 m upstream of the air pocket. PT3 was located 6.30 m downstream of the air pocket, while PT4 was located at the air pocket.

Previous work into transient interactions with in-line air (Kim 2008) (Pozos-Estrada 2017) has generally focused on transients generated by flow stoppage, and has therefore used a sudden valve closure to interrupt base flow and generate a compression wave. However, as the air in this investigation is located in the main flow path, tests were carried out with no base flow to prevent air being pushed from the system, moved to another location, or sheared by the flow. Therefore, the transient was generated via a rapid opening and closure of the electronically controlled solenoid valve, with the sudden start and stop of flow causing an expansion pulse which propagates back and forth along the pipeline. The pressure response was recorded at the four transducers for five seconds from the opening of the valve, enough time for the transient to dissipate entirely. Based on the wave speed measured for the system (1348.5 m/s), a, and the length of the pipe, L, this corresponds to approximately 167 cycles, where the pipeline period $T = \frac{4L}{a}$.

As well as the no-air pipe case, fourteen air pocket volumes were tested, ranging from 2.9 ml to 40 ml at atmospheric pressure ($V = \{2.9; 3.5; 7.1; 7.8; 9.9; 11.3; 15.5; 16.0; 16.5; 21.6; 26.5; 33.9; 34.6; 40.0\}$ ml). These volumes are below 2% of the total pipe volume, so could realistically occur as a result of air vaporisation. Tests were run for each air pocket volume at initial hydrostatic pressures ranging between 0.5 bar and 3.0 bar in 0.5 bar increments. The pocket volumes used range from a very small collection of air which barely obstructs the flow, to pockets which almost entirely block the crest at low initial hydrostatic pressures. This range of scenarios could realistically occur in a pipeline and provides a comprehensive study of the effect of an air pocket in a pipe system. To assess experimental error, testing was repeated ten times for each set of experimental conditions.

The standard error between the ten tests was observed to be less than 0.05% of the absolute pressure readings on average. To ensure no air became trapped elsewhere in the system, the pipe was bled at several side discharge valves along its length after each pressure increase and a period of sustained base flow with the upstream valve open was applied between each air pocket test.

The Baccara solenoid valve was programmed to open and close over a period of 6 ms. The control system for the valve was designed and made at the University of Canterbury. Based on the experimental wave speed determined for the system, the closure time of 6 ms corresponds to a pulse length of approximately 8.1 metres, or 20% of the total pipe length ($0.2L$). The pulse length provides an indication of the level of interference that may be expected in the pressure trace. As the pulse is shorter than the pipe itself, the reflections from the air pocket and system boundaries will not immediately blend together, allowing the extraction and analysis of individual pulses.

NUMERICAL MODELLING

Governing Equations

The results of a simple numerical model for the air-water interaction will be used to carry out an energy balance for the system. A 1D model is required to complete the energy balance. The air pocket volumes to be tested are small enough that the elastic water model is applicable, and the movement of the air-water interface does not need to be considered (Chaiko and Brinckman 2002). The Method of Characteristics (MOC) scheme is used to solve the mass and momentum conservation equations which govern 1D unsteady pipe flow (Wylie et al. 1993)

$$\frac{\partial V}{\partial t} + g\frac{\partial H}{\partial x} + gh_f = 0\,, \tag{1}$$

$$\frac{\partial H}{\partial t} + \frac{a^2}{g}\frac{\partial V}{\partial x} = 0\,, \tag{2}$$

where H is the piezometric head, V the fluid mean velocity, x the distance along the pipe, t the time, g acceleration due to gravity, and h_f the friction loss per unit length including both steady and unsteady components. The value of a was assumed to be constant along the whole pipe. Eqs. 1

and 2 are reduced to a set of characteristic equations by the MOC scheme, which can be solved simultaneously for the head $H_{i,j}$ and flow velocity $U_{i,j}$ at the end of time step j at a given node i in the MOC grid. The MOC grid was split into 180 spatial nodes distributed evenly along the pipe, with the time step selected to ensure the Courant number ($\frac{a\Delta t}{\Delta x}$) is fixed at unity. Sensitivity testing with a range of discretizations showed that the size of the spatial grid had only a minor impact on the solution compared to the additional computational time required. For example, increasing the discretization to 1000 nodes results in an average difference of less than 1% in the pressure pulse amplitudes predicted.

For high-speed transients, inaccuracies can arise in model predictions of energy loss and phase shift as a result of the changing velocity profile, turbulence, and laminar-turbulent transitions. The inclusion of unsteady friction in the model accounts for this effect. The methodology developed by Zielke (1968) was used for calculating friction terms

$$h_{f,(i,j)} = \frac{32\nu}{gD^2}V_{i,j} + \frac{16\nu}{gD^2}\sum_{k=1,3,..}^{j-1}(V_{i,j-k+1} - V_{i,j-k-1})W(j\Delta t)\,, \tag{3}$$

where h_f is the total friction loss including both unsteady and steady friction, D the pipe diameter, ν the kinematic viscosity of the fluid, and W a weighting function based on the dimensionless time which can be found in Zielke (1968). The method accounts for the velocity history of the given node as well as the current flow velocity. The method and Zielke's weighting function are suited to laminar flow regimes. The lack of base flow in the experimental system means that the flow velocities generated are small, and will satisfy this requirement.

Accumulator Model

The accumulator model incorporates an air pocket of a selected volume at a given nodal point. It is assumed that there is no column separation, i.e., the air does not occupy the full cross section of the pipe. This assumption was used by Burrows and Qiu (1995) in a previous numerical study, and the air volumes tested satisfy such an assumption. In addition, the initial hydrostatic pressure is high and the generated pressure disturbance is small relative to this, and therefore column separation is unlikely to occur. The pressure within the air pocket at any instant is assumed to be the same throughout the air pocket volume, and the compressibility of the liquid in the computational reach containing the air pocket is considered to be negligible compared to the compressibility of the air (Wylie et al. 1993). The polytropic relationship can be written at the end of the time interval Δt as

$$(H_A - z)(\forall + \Delta\forall)^n = C_A \,, \tag{4}$$

where H_A is the absolute head at the pocket, z the elevation of the pipe above the datum, $\forall$ the pocket volume at the beginning of the time interval Δt, $\Delta\forall$ the volume change across the time interval, n the polytropic exponent, and C_A the polytropic constant. Applying continuity principles, the volume change can be expressed as

$$\Delta\forall = \frac{2\Delta t}{\pi D^2}[(V_{i+1,j-1} - V_{i-1,j-1}) + (V_{i+1,j} - V_{i-1,j})] \,, \tag{5}$$

Combining the characteristic equations, the polytropic relationship, and Eqs. 4 and 5 yields a non-linear equation with H_P as the only unknown which can be solved using a root-finding algorithm.

Energy Equation

The energy equation (Karney 1990) (Karney et al. 2015) (Duan et al. 2017) will be used to assess the energy balance in the system. The energy equation is

$$\frac{dU}{dt} + \frac{dU_a}{dt} + \frac{dT_e}{dt} + D' + W' = 0 \,, \tag{6}$$

where U is the internal energy, U_a the elastic energy stored by the air pocket, T_e the kinetic energy, D' the rate of viscous energy dissipation, and W' the rate at which work is done on the fluid at each boundary. The extended versions of these terms can be found in Karney (1990) and Karney et al. (2015). The fluid pressure and velocity, evaluated numerically for each spatial node at each time step, are used to evaluate the energy balance for each time step. The equation may also be used to calculate the total energy in each form at each time step.

RESULTS

Experimental Results

Time Domain Observations

The experimental investigation involved the collection of pressure measurements at the transient generation point, upstream of the air pocket, and downstream of the air pocket. Thus it is possible to assess the properties of both the reflected and transmitted waves. Figs. 2 and 3 show traces measured at PT1, (the transient generation point), PT2 (6.21 m upstream of the pocket), PT4 (at the air pocket section), and PT3 (6.30 m downstream of the pocket) for a set of representative air volumes. The approximate obstruction created by each air volume for the 3.0 bar scenario is shown in Fig. 4. The pressure traces presented have been normalised by the initial hydrostatic pressure such that $H^* = \frac{H}{H_0}$, where H is the measured gauge pressure at any time and H_0 is the steady state initial hydrostatic pressure. The elapsed time since the start of the transient event t is normalised by the pipeline period T, such that $t^* = \frac{t}{T}$.

In the experiments, the air pocket volumes were measured outside the pipe at atmospheric pressure before and after each test using a measuring syringe. This volume is converted to a pressurised volume inside the pipe using the reversible polytropic relation, $H_A \forall^n = C_A$. The polytropic exponent may range between 1.0 and 1.4, but an average value of 1.2 has been commonly used in previous research on air-water interactions (Martin 1976) (Wylie et al. 1993) (Izquierdo et al. 1999) (Carlos et al. 2011), and is used here. Using this equation, the volumes measured at atmospheric pressure can be converted into steady state volumes within the pipe once pressurised. The steady state in-pipe volumes are then converted to a length scale, as this can be used to understand the compression behaviour of the pocket. In Figs. 2 and 3, the pocket length scale, L_P, is approximated as $L_P \sim \forall^{\frac{1}{3}}$. L_P is normalised by the length of the pipe such that $L_P^* = \frac{L_P}{L}$. The work done on the pocket by the transient wave scales as $PA_PV_PT_P$, where P is the pressure on the pocket, A_P the pocket surface area, V_P the radial velocity of the air-water interface, and T_P the duration of the compression phase. When the compression length scale (V_PT_P) is less than the pocket length scale (L_P), the pocket is compressed but does not collapse. When the compression length scale is longer than the pocket length, the pocket collapses, resulting in large pressure spikes. Examples of this scenario include the experiments by Jönsson (1985) and Lee and Martin (1999) which observed peak pressure enhancements of four or five times the initial hydrostatic pressure.

Figs. 2 and 3 show that the partial reflections occurring at the pocket result in significantly more pressure peaks in the transient trace than observed in the no-air case. For instance, by $t^* \approx 0.5$, the arrival time of the first reflected pulse at the upstream sensor (PT2) for the no-air case, four pulses have arrived at PT2 for the air pocket scenarios. While the first reflected and transmitted pulses are fairly clear, as boxed in Figs. 2 and 3, interference patterns develop beyond $t^* \approx 0.3$ as reflections from the air pocket and the ends of the system begin to interfere with each other. As boxed in Figs. 2 and 3, the reflected pulse is followed by a low pressure peak and extended tail which gradually levels off towards zero. From a diagnostic standpoint, Meniconi et al. (2016) has shown that this effect is not unique to the in-line air pocket, and a pressure drop following the reflected pulse may also be observed for solid blockage situations where the path of the pressure wave around the blockage is almost straight.

It is also worth noting that the pressure trace for the smallest pocket length varies significantly from the other three traces, which follow each other reasonably closely. This suggests that below a certain pocket volume threshold small changes in pocket volume begin to have a more significant effect on the transient behaviour, or the dominant physical processes of the transient-air interaction begin to change. This may be explained by the underlying physical theory of the interaction. Continuity and momentum theory state that

$$\frac{d\forall}{dt} = Q_a \tag{7}$$

$$\frac{dH_a}{dx} = 0 \tag{8}$$

where Q_a is the flow rate at the air-fluid interface due to the volume change of the air pocket under the transient pressure condition. Eqs. 7 and 8 state that any change in the air pocket volume results in a corresponding change to the system flow rate, and that the pressure of the air pocket is homogeneous. Differentiating the polytropic equation and applying Eq. 7 gives

$$\frac{dH_a}{dt} = -\frac{nH_a}{\forall} Q_a \tag{9}$$

Consequently, the transient variation of the hydraulic properties, pressure and flow rate, depend on the volume of the pocket as well as the instantaneous pressure state. If the above equation is considered in terms of the transient fluctuations in pressure and volume, it becomes

$$\frac{dh_a}{dt} = -\frac{n}{\forall_0 + \forall_t} Q_a \tag{10}$$

where h_a is the transient fluctuation in pressure, $\forall_0$ is the steady state pocket volume, and $\forall_t$ is the transient fluctuation in pocket volume. Therefore it can be concluded that for large pockets, where transient volume changes are small relative to the steady state air volume, the transient behaviour is largely dependent on the initial state of the air pocket ($\forall_0$). Meanwhile, for relatively small pockets, where volume fluctuations are significant compared to the steady state volume, the transient behaviour is instead dependent on the instantaneous change in air pocket volume ($\forall_t$). The results of the accumulator model were used to check the expected volume fluctuations for each experimental case. The smallest pocket sizes tested, which display a very different transient response, experience considerably greater relative volume changes than the mid- to upper- range of volumes. For instance, for the 3.0 bar case the two smallest volumes experience relative volume changes of approximately 10% of the starting volume, compared to other pocket volumes where the relative volume change is less than 5%. This observation may therefore be attributable to the changing air-transient dynamics as pocket volume is reduced.

The pressure traces indicate that increasing the air pocket size increases the amplitude of the reflected pressure pulses and decreases the amplitude of the transmitted pulses. This can be explained by impedance theory. The impedance, Z, of a pipe is given by $Z = \frac{\rho a}{A}$ where ρ is the fluid density and A is the cross-sectional area of the pipe (Gong et al. 2013). It can be used to determine the reflection coefficient, RC, which is the amplitude of the reflected pulse relative to the amplitude of the incident pulse. It is defined as $RC = \frac{Z_A - Z_0}{Z_A + Z_0}$ where Z_A is the impedance of the pipe section containing the air pocket and Z_0 is the impedance of the pipe without the air pocket. Z_A is smaller than Z_0, due to the low density of the air and the local reduction in wave speed caused by the air's compressibility. As the size of the air pocket increases, Z_A decreases, therefore increasing the absolute value of RC in agreement with experimental observations. In addition, the theoretical RC is negative, accounting for the out of phase reflection observed. This phase change is the opposite of what would be observed for a solid flow constriction, which has a greater impedance than the clear pipe. This is a useful point of difference which may be utilised in diagnostic testing when a loss of flow or increase in pumping costs is observed in the system.

Reflection and Transmission Coefficients

Reflection and transmission coefficients provide a quantitative measure of the air pocket's effect on the incident transient pulse. These coefficients are calculated as

$$RC = \frac{H_R}{H_I} - \frac{H_{R,0}}{H_{I,0}} , \tag{11}$$

$$TC = \frac{H_T}{H_I} , \tag{12}$$

where RC is the reflection coefficient, TC the transmission coefficient, H_I the peak amplitude of the incident pulse measured upstream of the pocket at PT2, H_R the peak amplitude of the first reflected pulse measured upstream of the pocket at PT2, and H_T the peak amplitude of the first transmitted pulse measured downstream of the pocket at PT3. Small reflections were observed from the crest section for the no-air case. To clearly identify the effect of the injected air on the response, a reflection coefficient was calculated for the no-air case at each initial hydrostatic pressure $(\frac{H_{R,0}}{H_{I,0}})$ and subtracted from the reflection coefficients calculated for the air pocket cases $(\frac{H_R}{H_I})$ at that initial hydrostatic pressure. The values used in the calculation are marked on example pressure traces in Fig. 5.

The reflection and transmission coefficients for each steady state pressurised pocket length are shown in Figs. 6 and 7. Sensitivity testing showed that the general trends observed are independent of the polytropic constant used to obtain the steady state air length within the pipe, and the standard error in RC and TC due to experimental variation is approximately 2%. For the no-air case TC is slightly less than 1, indicating that there is a small quantity of energy loss across the 12.85 m pipe section between PT2 and PT3 when air is not present. In accordance with impedance theory introduced previously, the absolute value of RC increases with pocket length. The experimental RC values are in agreement with those estimated using the theoretical equations introduced previously, particularly for the upper range of pocket sizes. The average error is less than 4%, as shown in Fig. 8. The theoretical values for RC were calculated using a weighted average density for the crest section, and a wave speed at the crest section estimated using the void ratio of the crest section and the wave speed equation presented by Lee (1991).

The range of RC and TC observed can be compared to the values expected for solid blockages under similar conditions. Solid flow blockages generate reflections with an amplitude dependent on the base flow of the system, with severe flow constrictions required to generate significant reflections under zero base flow. The smallest air pocket volumes block only approximately 6% of the total pipe cross-section, but generate reflections under zero base flow comparable to solid blockages which almost entirely block the pipe cross-section (Meniconi et al. 2011). This is a useful diagnostic property of the air pocket. If flow loss is observed in an operational pipeline, it can be tested under zero base flow conditions and the amplitude of the transient reflection compared to the degree of flow loss observed when operational to differentiate between air pockets and solid blockages.

As discussed previously, past studies have observed reflected peak amplitudes which significantly exceed the initial hydrostatic pressure due to pocket collapse. For this set of experiments, the sum of RC and TC reached a maximum of approximately 1.2. The duration of the original transient pulse used in this work (6 ms) is approximately two orders of magnitude less than the compression duration used in Jönsson (1985) and Lee and Martin (1999) ($T_P \sim 0.5$ - 3 s). The base flows of approximately 1 m/s applied in Jönsson (1985) and higher driving pressures of up to 8 bar in Lee and Martin (1999) also result in higher radial velocities. The maximum velocities predicted by the numerical model for this experimental case are in the order of 0.1 m/s. Meanwhile, the pocket length scales used by Jönsson (1985) and Lee and Martin (1999) (L_P ~0.4 - 0.8 m) are only approximately one order of magnitude greater than those used here (L_P ~0.02 m). Therefore the size of the compression length scale relative to the initial pocket length is much smaller than was used for the above studies. The lack of base flow and the short duration of the original transient pulse mean the compression scale is too small to result in pocket collapse and, unlike previous studies, large pressure spikes are not observed.

Spectral Analysis

The shapes of the incident, reflected, and transmitted pulses are quantified using their frequency content, calculated using a direct Fourier transform (DFT). This method enables both the main peaks and the extended tails of the reflected and transmitted pulses to be included in the analysis. However, the experimental trace is subject to interference from ongoing reflections and in the majority of cases the low pressure tail is interrupted by the arrival of further reflections, as shown in Figs. 2 and 3. It was necessary to artificially generate data points to complete the pulses, with the placement of these additional points based on the shape of the preceding data and modelled pulses generated using non-reflecting boundary conditions. Sensitivity testing indicated that while artificial points completing the tail were required to achieve a reasonable result, small variations in their placement did not have a significant effect on the shape of the DFT obtained.

Fig. 9 shows the DFT amplitude for the frequencies contained in the incident and resultant pulses for a set of representative air lengths. The DFT amplitude is normalised by the initial hydrostatic pressure ($h^* = \frac{h}{H_0}$), while the frequency is normalised by the inverse of the pipeline period ($\omega^* = T\omega$). Several key trends are visible in the DFTs for the particular pocket length, configuration, and pressure disturbance used. The upper range of frequencies ($\omega^* \approx 20 - 70$) contained in the incident pulse are present in the reflected pulse at approximately the same amplitude (within 4%). In the transmitted pulse the amplitude of this frequency range is approximately 3%

of the incident amplitude, meaning the upper range of frequencies contained in the incident pulse is primarily reflected back by the air pocket. This frequency dependent transmissivity is due to the compressibility of the air, and has previously been observed in the field of acoustics (Domenico 1982) (Leighton et al. 1998). Significant reductions in transmissivity are observed for signal frequencies above the air pocket's resonant frequency, and this frequency content is reflected back by the air. Calculating the resonant frequency for an in-line air pocket is difficult due to the unknown geometry of the pocket (Jang et al. 2009). However, for the off-line pocket case, where the geometry is known, the DFT agrees with theoretical predictions of the resonant frequency, as ascertained by the authors in yet to be published research. The frequency dependent behaviour has therefore been quantified using a cut-off frequency for transmission by the air pocket, defined here as the frequency where the amplitude of the transmitted pulse DFT is first less than 5% of the amplitude of the incident pulse DFT. The cut-off frequencies are marked with vertical lines on Fig. 9. The cut-off frequency decreases with increasing air volume, consistent with theoretical expectations for the resonant frequency (Jang et al. 2009). This effect is not observed for other pipeline anomalies such as solid blockages and leaks, which do not impose a significant change in shape on the incident pulse during reflection and transmission (Brunone 1999) (Meniconi et al. 2011).

It was expected that the DFTs of the reflected and transmitted pulses would form smooth curves with reduced amplitude relative to the incident pulse for the entire frequency range. However, at larger pocket lengths there is some irregularity in the DFT of the reflected pulse for $\omega^* \lesssim 10$. There is also an increase in the amplitude of the reflected and transmitted frequencies above that of the incident pulse for $\omega^* \lesssim 5$. In the time domain, the low pressure tails of the reflected and transmitted pulses for a large pocket display many small fluctuations and are of long duration. This is the likely source of the irregularities observed in the low frequency response, though the physical reasoning for this is unclear, with further numerical and experimental analysis needed.

Transmission and reflection coefficients can be calculated in the frequency domain by comparing the DFT amplitudes for the transmitted and reflected pulses to the DFT amplitude of the incident pulse at each frequency:

$$RC_\omega = \frac{h_{R,\omega}}{h_{I,\omega}} \quad (13)$$

$$TC_\omega = \frac{h_{T,\omega}}{h_{I,\omega}} \quad (14)$$

where RC_ω and TC_ω are the reflection and transmission coefficients for a given frequency, ω, and $h_{I,\omega}$, $h_{R,\omega}$, and $h_{T,\omega}$ are DFT amplitudes of the incident, reflected and transmitted pulses at that frequency. Summing the squares of RC_ω and TC_ω at each frequency gives a measure of the energy contained in the reflected and transmitted pulses relative to the incident pulse, and therefore of the energy amplification or dissipation which occurs during the reflection and transmission process. Fig. 10 shows the total energy contained in the reflected and transmitted pulses at each frequency relative to the incident pulse for four representative air lengths. The relative energy ranges between 0.85 and 1 for $\omega^* \gtrsim 5$. The average relative energy across the range of frequencies in the reflected and transmitted pulses is also less than 1 for the cases tested, despite the amplification observed at low frequencies. This indicates that energy losses occur between the incident pulse and the reflected and transmitted pulses generated by the pocket. This may be explained by the energy balance theory introduced previously. The results of the numerical model provide a fair match to the experimental data, with example predictions for the pressure traces measured upstream and downstream of the pocket shown in Fig. 11. There are noticeable discrepancies in the wave amplitudes and arrival times, but the results of the model can be used to obtain a general representation of the distribution of system energy between kinetic, internal, air storage, and viscous dissipation forms. Fig. 12 shows the variation in the kinetic, internal, and air storage energy of the system for $t^* = 0-1.5$. The energies are scaled by the initial energy stored by the air pocket ($E^* = \frac{E}{U_{a,0}}$). Viscous dissipation accounts for less than 2% of the system's kinetic energy, and is therefore too small to be shown. The compressibility of the air and the lack of base flow in the system mean that the majority of the system energy is stored in the air pocket. Given that viscous dissipation is negligible within the time-frame of the first air-transient interaction, it is likely that the energy loss observed in the frequency domain is therefore attributable to conversion to air pocket storage during the compression and expansion phases.

Effects of Initial Hydrostatic Pressure

Initial hydrostatic pressure has been shown to have an effect on the transient trace for the dead-end pocket scenario (Zhou et al. 2002) and the brass block case (Kim 2008). The RCs and TCs calculated previously provide a quantitative assessment of the effects of initial hydrostatic pressure on the in-line pocket interaction with the transient. Fig. 7 shows that for the no-air case TC increases as the initial hydrostatic pressure is increased, however the total range of TC for the no-air case is less than 0.02. For larger air lengths ($L^* \gtrsim 0.06$), Figs. 6 and 7 show that the variation in RC and TC with initial hydrostatic pressure is comparable to the no air case. However, the effect of initial hydrostatic pressure on the reflected and transmitted pulse amplitude becomes increasingly significant as the air length is reduced below this threshold. This suggests that when assessing the size of entrapped air pocket from transient reflections and transmissions the initial hydrostatic pressure should be taken into account.

Inspection of the DFTs for air pockets which occupy a similar length when compressed to different initial hydrostatic pressures suggests there is no relationship between initial hydrostatic pressure and DFT amplitude. This also applies to the cut-off frequency observed for the transmitted pulse, suggesting it is only influenced by the size of the pocket but not the initial hydrostatic pressure for the given experimental conditions. These findings are useful in a diagnostic scenario under similar conditions as the air pocket size may be estimated from the cut-off frequency alone.

CONCLUSIONS AND RECOMMENDATIONS

Controlled experimental investigations are needed to distinguish the effects of entrapped in-line air pockets on fluid transients. The purpose of this study was to present experimental data for the in-line air pocket case under realistic system conditions and to characterise the effects of air on the transient in terms of reflection and transmission. To assist in developing a diagnostic framework, it is useful to note how the effects of air compare to other faults which cause a flow constriction at steady state. Air pockets can often be cheaper to remove than solid blockages, meaning it is advantageous to be able to differentiate between the two cases when flow loss is observed.

The experimental results show that the reflective power of the air pocket increases with its length, in agreement with impedance theory. Though the low pressure tail following the transient reflection may also be observed for a solid blockage, the out-of-phase reflection from the flow constriction is unique to the air pocket. Unlike a solid blockage, air pockets also result in a sizeable reflection under zero base flow conditions regardless of the degree of cross-section blockage. Linking the amplitude of the transient reflection under zero base flow to the observed flow loss during operation can therefore be used to differentiate between air and solid blockages.

Analysis in the frequency domain shows that the air pocket transmits only the lower range of frequencies contained in the incident pulse, with the upper range of frequencies being primarily reflected. This frequency dependent transmissivity is also unique to air among flow-blocking elements. The transmission cut-off frequency decreases as pocket length increases, similar to the theoretical resonant frequency of trapped air. The reflection and transmission coefficients calculated in the frequency domain also indicate that, on average, the incident pulse loses energy over the range of frequencies contained within it during reflection and transmission. An investigation of energy distribution within the system indicated that this energy loss is likely to be due to conversion to air pocket storage.

Six different initial hydrostatic pressures were used in the experimental tests to assess the effects of steady state pressure on the transient behaviour. As the air length is reduced, the effect of initial hydrostatic pressure on the amplitude of the transmitted and reflected pulses becomes increasingly significant.

DATA AVAILABILITY STATEMENT

Some or all data, models, or code generated or used during the study are available from the corresponding author by request.

ACKNOWLEDGEMENTS

We would like to thank Hong Kong Research Grants Council for the theme based research

scheme (TRS) Grant No. T21-602/15R for supporting this research.

NOTATION

The following symbols are used in this paper:

a	=	wave speed
A	=	pipe cross-sectional area
A_P	=	air pocket surface area
C_A	=	polytropic constant
D	=	pipe diameter
D'	=	viscous energy dissipation rate
E	=	energy
g	=	gravitational acceleration
h	=	DFT amplitude
h_{f}	=	total friction loss
H	=	piezometric head
i	=	spatial index
j	=	temporal index
L_p	=	pocket length scale
L	=	pipe length
n	=	polytropic exponent
P	=	air pocket pressure
Q	=	flow rate
RC	=	reflection coefficient
t	=	time
Δt	=	computational time step
TC	=	transmission coefficient
T	=	pipeline period
T_e	=	kinetic energy

T_P = duration of pocket compression

$\mathcal{V}$ = air pocket volume

V = fluid velocity

V_P = radial velocity of the air-water interface

U = internal energy

U_a = energy stored by air pocket

W = unsteady friction weighting function

W' = boundary work rate

x = longitudinal distance

z = elevation

Z = impedance

ν = kinematic viscosity

ρ = density and

ω = frequency.

REFERENCES

Auditor-General (2010). *Local authorities: Planning to meet the forecast demand for drinking water*. New Zealand Government.

Brunone, B. (1999). "Transient test-based technique for leak detection in outfall pipes." *Journal of Water Resources Planning and Management*, 125(5), 302–306.

Burrows, R. and Qiu, D. (1995). "Effect of air pockets on pipeline surge pressure." *Proceedings of the Institution of Civil Engineers-Water, Maritime, and Energy*, 112(4), 349–361.

Cabrera, E., Abreu, J., Pérez, R., and Vela, A. (1992). "Influence of liquid length variation on hydraulic transients." *Journal of Hydraulic Engineering*, 118(12), 1639–1650.

Carlos, M., Arregui, F., Cabrera, E., and Palau, C. (2011). "Understanding air release through air valves." *Journal of Hydraulic Engineering*, 137(4), 461–469.

Chaiko, M. and Brinckman, K. (2002). “Models for analysis of water hammer in piping with entrapped air.” *Journal of Fluids Engineering*, 124(1), 194–204.

Domenico, S. (1982). “Acoustic wave propagation in air-bubble curtains in water—Part I: History and theory.” *Geophysics*, 47(3), 345–353.

Duan, H., Meniconi, S., Lee, P., Brunone, B., and Ghidaoui, M. (2017). “Local and integral energy-based evaluation for the unsteady friction relevance in transient pipe flows.” *Journal of Hydraulic Engineering*, 143(7), 04017015.

Fuertes, V., Cabrera, E., Izquierdo, J., and Iglesias, P. (1999). “Peak pressure evaluation in pipelines with entrapped air pockets.” *Proceedings of the 3rd ASME/JSME Joint Fluids Engineering Conference, San Francisco, USA*.

Gong, J., Simpson, A. R., Lambert, M. F., Zecchin, A. C., Kim, Y.-i., and Tijsseling, A. S. (2013). “Detection of distributed deterioration in single pipes using transient reflections.” *Journal of Pipeline Systems Engineering and Practice*, 4(1), 32–40.

Izquierdo, J., Fuertes, V., Cabrera, E., Iglesias, P., and Garcia-Serra, J. (1999). “Pipeline start-up with entrapped air.” *Journal of Hydraulic Research*, 37(5), 579–590.

Jang, N. W., Gracewski, S. M., Abrahamsen, B., Buttaccio, T., Halm, R., and Dalecki, D. (2009). “Natural frequency of a gas bubble in a tube: Experimental and simulation results.” *The Journal of the Acoustical Society of America*, 126(1), EL34–EL40.

Jönsson, L. (1985). “Maximum transient pressures in a conduit with check valve and air entrainment.” *International Conference on the Hydraulics of Pumping Stations*, 55–76.

Karney, B., Malekpour, A., and Nault, J. (2015). “Metrics for the rapid assessment of transient severity in pipelines.” *Pipelines 2015*, 815–824.

Karney, B. W. (1990). “Energy relations in transient closed-conduit flow.” *Journal of Hydraulic Engineering*, 116(10), 1180–1196.

Kim, Y. I. (2008). “Advanced numerical and experimental transient modelling of water and gas pipeline flows incorporating distributed and local effects.” Ph.D. thesis, University of Adelaide, University of Adelaide.

Lai, A., Hau, K., Noghrehkar, R., and Swartz, R. (2000). "Investigation of waterhammer in piping networks with voids containing non-condensable gas." *Nuclear Engineering and Design*, 197(1-2), 61–74.

Lauchlan, C., Escarameia, M., May, R., Burrows, R., and Gahan, C. (2005). "Air in pipelines." *HR Wallingford. Report SR*, 649.

Lee, N. and Martin, C. (1999). "Experimental and analytical investigation of entrapped air in a horizontal pipe." *Proceedings of the 3rd ASME/JSME Joint Fluids Engineering Conference, July*, 18–23.

Lee, N. H. (2005). "Effect of pressurization and expulsion of entrapped air in pipelines." Ph.D. thesis, Georgia Institute of Technology, Georgia Institute of Technology.

Lee, T. (1991). "Numerical computation of fluid pressure transients in pumping installations with air entrainment." *International Journal for Numerical Methods in Fluids*, 12(8), 747–763.

Leighton, T., Ramble, D., Phelps, A., Morfey, C., and Harris, P. (1998). "Acoustic detection of gas bubbles in a pipe." *Acta Acustica united with Acustica*, 84(5), 801–814.

Martin, C. (1976). "Entrapped air in pipelines." *Proceedings of the 2nd International Conference on Pressure Surges*, Vol. 2, British Hydromechanics Research Association Bedford, UK, 15–27.

Meniconi, S., Brunone, B., and Ferrante, M. (2011). "In-line pipe device checking by short-period analysis of transient tests." *Journal of Hydraulic Engineering*, 137(7), 713–722.

Meniconi, S., Brunone, B., Ferrante, M., and Capponi, C. (2016). "Mechanism of interaction of pressure waves at a discrete partial blockage." *Journal of Fluids and Structures*, 62, 33–45.

National Research Council, N. (1982). *Drinking Water and Health: Volume 4*. The National Academies Press, Washington, DC.

Ocasio, J. (1976). "Pressure surging associated with pressurization of pipelines containing entrapped air." *Special MS Research Report*.

Pozos, O. (2007). *Investigation on the effects of entrained air in pipelines*. University of Stuttgart.

Pozos, O., Gonzalez, C. A., Giesecke, J., Marx, W., and Rodal, E. A. (2010). "Air entrapped in gravity pipeline systems." *Journal of Hydraulic Research*, 48(3), 338–347.

Pozos-Estrada, O. (2017). “Investigation of the combined effect of air pockets and air bubbles on fluid transients.” *Journal of Hydroinformatics*, 20(2), 376–392.

Spellman, F. R. (2013). *Handbook of water and wastewater treatment plant operations*. CRC press.

Vasconcelos, J. G. and Leite, G. M. (2012). “Pressure surges following sudden air pocket entrapment in storm-water tunnels.” *Journal of Hydraulic Engineering*, 138(12), 1081–1089.

Wylie, E. B., Streeter, V. L., and Suo, L. (1993). *Fluid transients in systems*, Vol. 1. Prentice Hall Englewood Cliffs, NJ.

Young, F. R. (1999). *Cavitation*. World Scientific.

Zhou, F. (2000). “Effects of trapped air on flow transients in rapidly filling sewers.” Ph.D. thesis, University of Alberta, University of Alberta.

Zhou, F., Hicks, F., and Steffler, P. (2002). “Transient flow in a rapidly filling horizontal pipe containing trapped air.” *Journal of Hydraulic Engineering*, 128(6), 625–634.

Zhou, L., Liu, D., Karney, B., and Zhang, Q. (2011). “Influence of entrapped air pockets on hydraulic transients in water pipelines.” *Journal of Hydraulic Engineering*, 137(12), 1686–1692.

Zielke, W. (1968). “Frequency-dependent friction in transient pipe flow.” *Journal of Basic Engineering*, 90(1), 109–115.

List of Figures

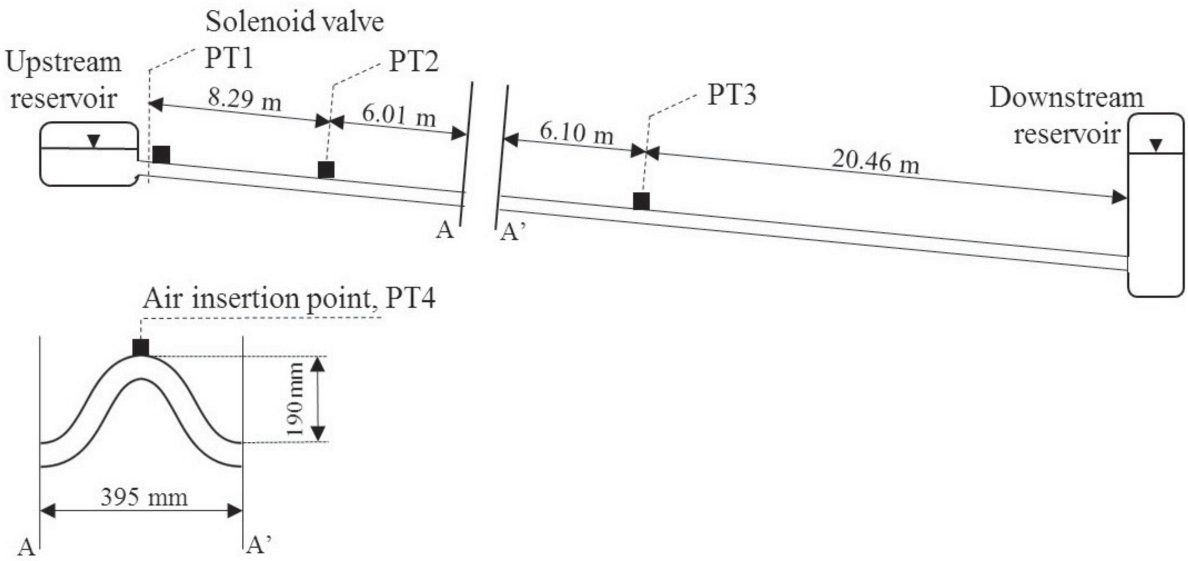

Fig. 1. Diagram of experimental set-up

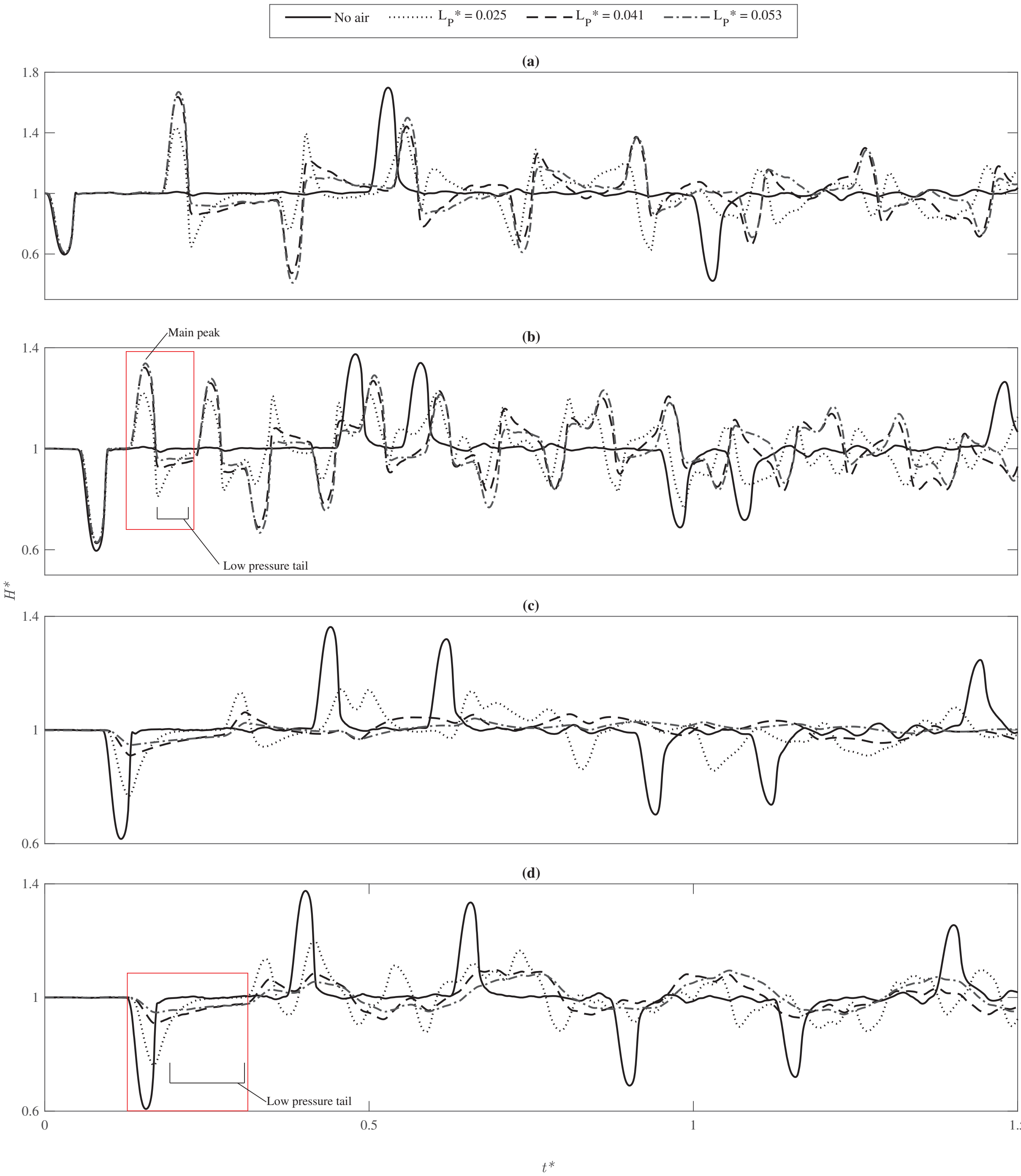

Fig. 2. Experimental pressure traces for a range of representative pocket lengths and the no-air case at an initial hydrostatic pressure of 3.0 bar (a) Pressure trace measured at PT1, at the transient generation point, (b) Pressure trace measured at PT2, upstream of the pocket, (c) Pressure trace measured at PT4, at the air pocket section, and (d) Pressure trace measured at PT3, downstream of the pocket. The first reflected and transmitted pulses are boxed in (b) and (d).

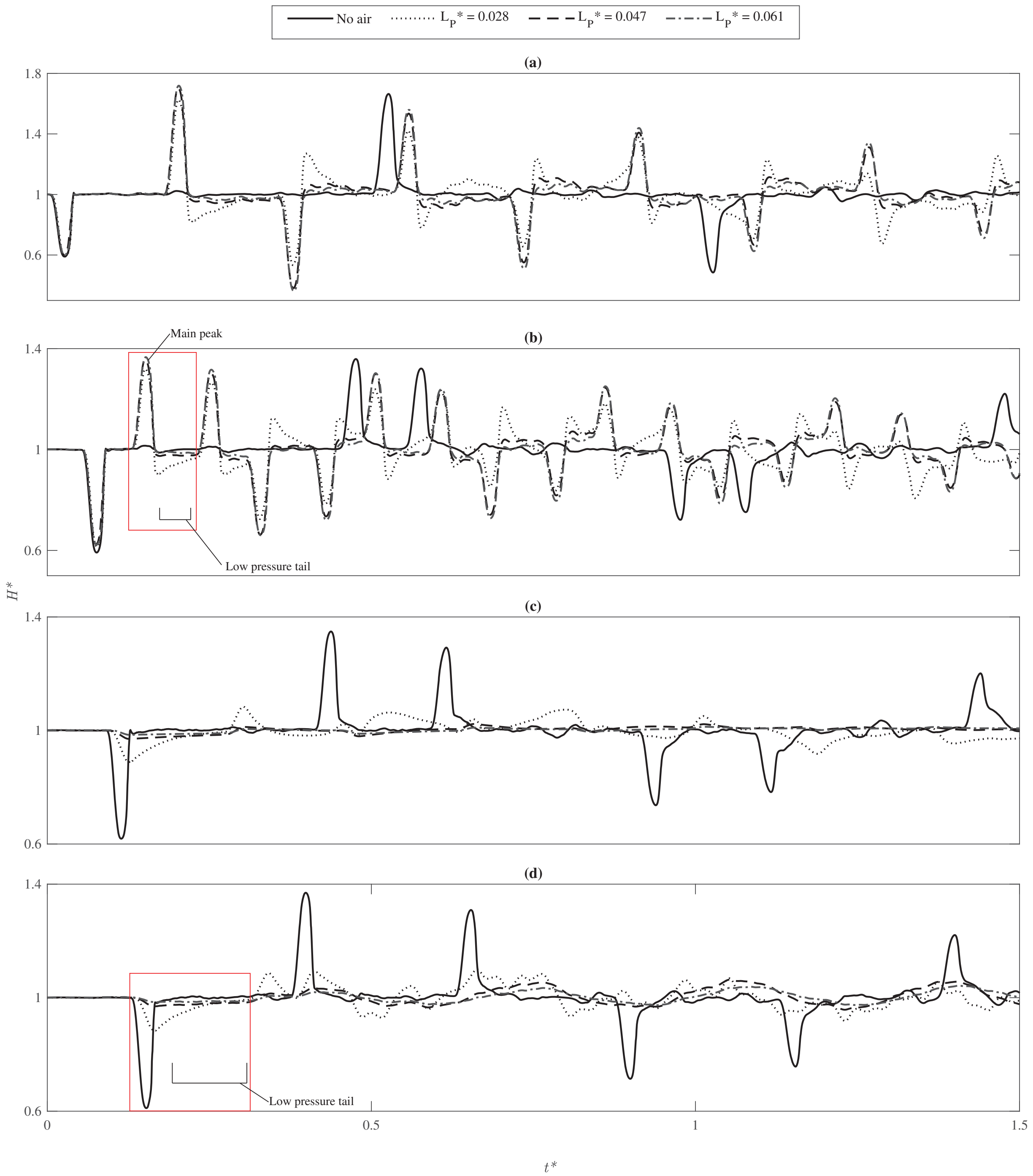

Fig. 3. Experimental pressure traces for a range of representative pocket lengths and the no-air case at an initial hydrostatic pressure of 1.5 bar (a) Pressure trace measured at PT1, at the transient generation point, (b) Pressure trace measured at PT2, upstream of the pocket, (c) Pressure trace measured at PT4, at the air pocket section, and (d) Pressure trace measured at PT3, downstream of the pocket. The first reflected and transmitted pulses are boxed in (b) and (d).

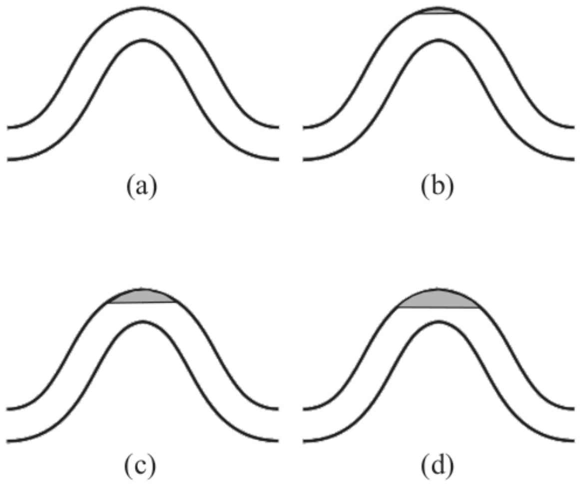

Fig. 4. Approximate obstruction caused by air pocket (shaded) pressurised to 3.0 bar for (a) No air, (b) $L_P^* = 0.025$, (c) $L_P^* = 0.041$, and (d) $L_P^* = 0.053$.

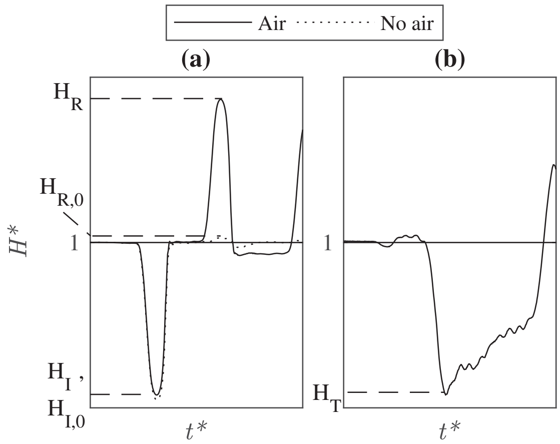

Fig. 5. Values used in calculation of reflection and transmission coefficients, a) Incident and reflected pulses measured at PT2, upstream of the pocket, b) Transmitted pulse measured at PT3, downstream of the pocket

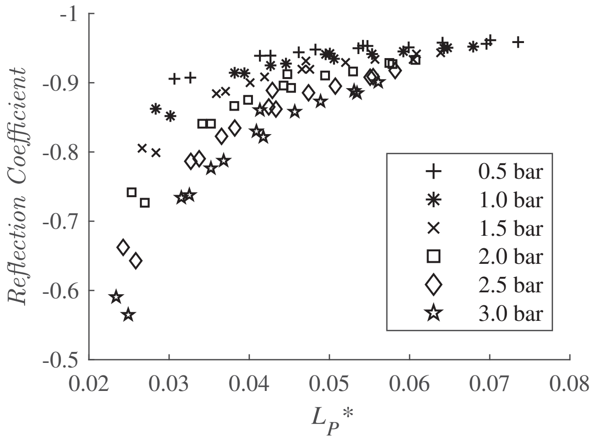

Fig. 6. Reflection coefficient of experimental pulses measured at PT2 for different initial hydrostatic pressures

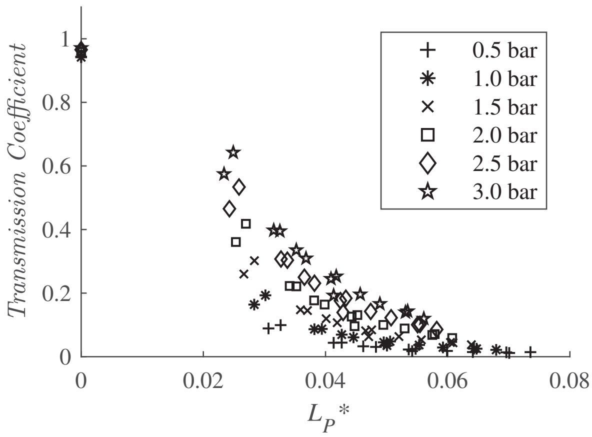

Fig. 7. Transmission coefficients of experimental pulses measured at PT3 for different initial hydrostatic pressures

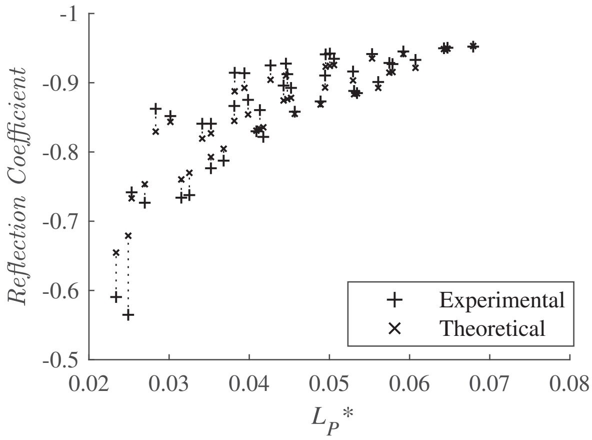

Fig. 8. Comparison of the reflection coefficients observed experimentally and predicted from theoretical equations. Corresponding air volumes are linked by dotted lines.

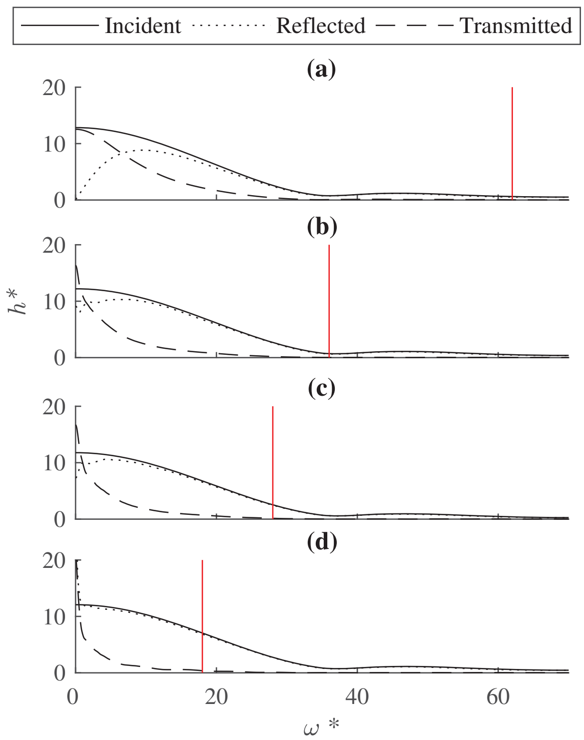

Fig. 9. DFT amplitude of incident, reflected, and transmitted pulses at an initial hydrostatic pressure of 3.0 bar for air pocket length (a) $L_P^* = 0.023$, (b) $L_P^* = 0.037$, (c) $L_P^* = 0.042$ (d) $L_P^* = 0.053$. Cut-off frequencies for the transmitted pulse DFT are marked by a vertical line.

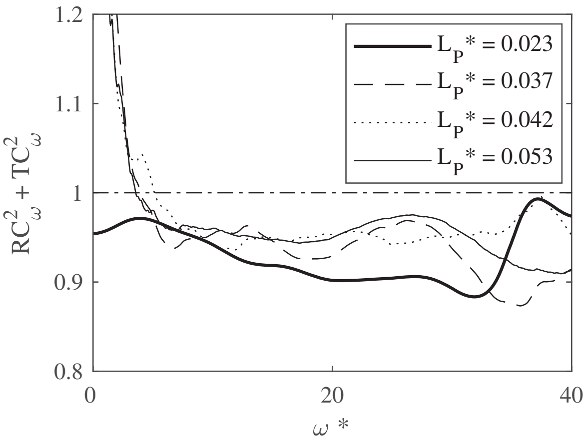

Fig. 10. Summed squares of reflection and transmission coefficients for frequencies contained within the incident pulse for air pockets at a initial hydrostatic pressure of 3.0 bar. A reference line is included at $RC_{\omega}^{2} + TC_{\omega}^{2} = 1$.

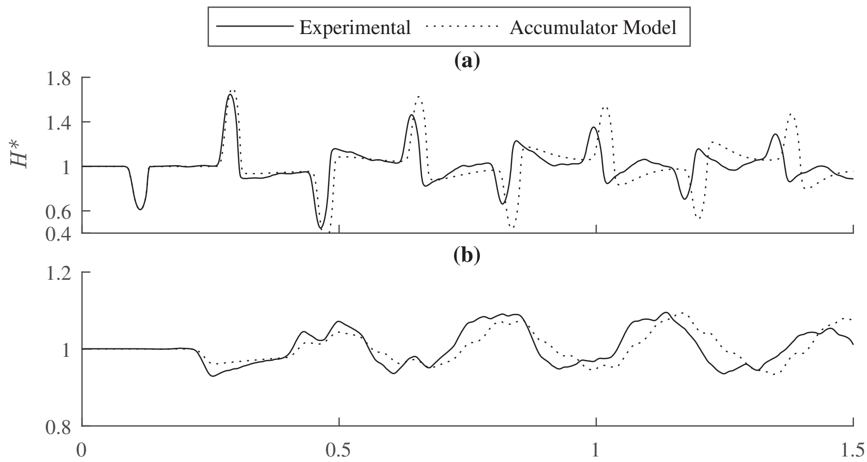

Fig. 11. Modelled and experimental pressure traces for $L_P^* = 0.042$ at 3.0 bar initial hydrostatic pressure (a) upstream of the pocket at PT2 and (b) downstream of the pocket at PT3

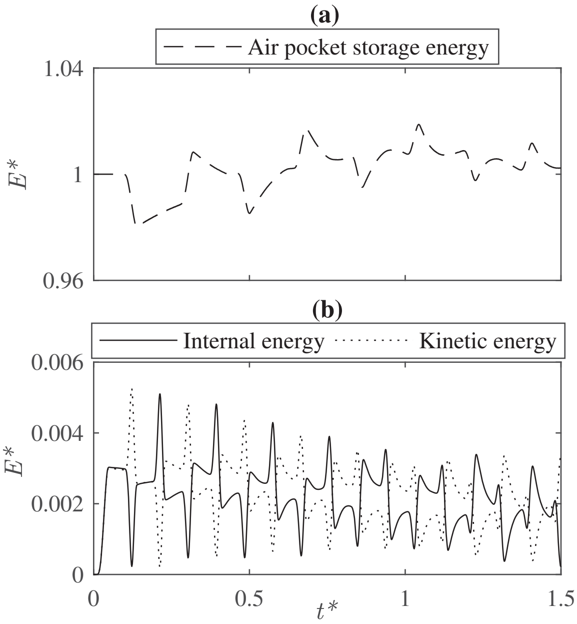

Fig. 12. Air storage, internal, and kinetic energy for $L_P^* = 0.042$ at 3.0 bar initial hydrostatic pressure